ELSEVIER

Journal of Fluids and Structures 24 (2008) 505–526

JOURNAL OF FLUIDS AND STRUCTURES

www.elsevier.com/locate/jfs

Strouhal numbers, forces and flow structures around two tandem cylinders of different diameters

Md. Mahbub Alam*, Y. Zhou

Department of Mechanical Engineering, The Hong Kong Polytechnic University, Hung Hom, Kowloon, Hong Kong, China

Received 7 February 2007; accepted 1 October 2007
Available online 3 December 2007

Abstract

This paper presents a detailed investigation of Strouhal numbers, forces and flow structures in the wake of two tandem cylinders of different diameters. While the downstream cylinder diameter, D, was fixed at 25 mm, the upstream cylinder diameter, d, was varied from $0.24D$ to D. The spacing between the cylinders was $5.5d$, at which vortices were shed from both cylinders. Two distinct vortex frequencies were detected behind the downstream cylinder for the first time for two tandem cylinders of the same diameter. The two vortex frequencies remained for $d/D = 1.0$–0.4. One was the same as detected in the gap of the cylinders, and the other was of relatively low frequency and was ascribed to vortex shedding from the downstream cylinder. While the former, if normalized, declined progressively from 0.196 to 0.173, the latter increased from 0.12 to 0.203 with decreasing d/D from 1 to 0.24. The flow structure around the two cylinders is examined in the context of the observed Strouhal numbers. The time-averaged drag on the downstream cylinder also climbed with decreasing d/D, though the fluctuating forces dropped because vortices impinging upon the downstream cylinder decreased in scale with decreasing d/D.

1. Introduction

The study of aerodynamic interference between two closely separated cylinders is of both fundamental and practical significance. In engineering, fluid forces and Strouhal numbers are the major factors to consider in the design of multiple slender structures subjected to cross-flow, e.g., chimney stacks, tube bundles in heat exchangers, overhead power-line bundles, bridge piers, stays, masts, chemical-reaction towers, offshore platforms and adjacent skyscrapers. The simplest configuration of multiple slender structures is two cylinders in either tandem or side-by-side arrangement. From the fundamental point of view, aerodynamic interference between two closely separated cylinders may give rise to flow separation, reattachment, vortex impingement, recirculation and quasi-periodic vortices, involving most generic flow features associated with multiple structures. Thus, flow around two cylinders provides a good model to understand the physics of flow around multiple cylindrical structures.

Flow around two tandem cylinders of identical cylinders is in general classified into three regimes (Zdravkovich, 1987): (i) the extended-body regime, where the two cylinders are so close to each other that the free shear layers separated from the upstream cylinder overshoot the downstream one, and the flow in the gap of the cylinders is

*Corresponding author. Tel.: +852 27667813; fax: +852 23654703.
E-mail address: mmalam@polyu.edu.hk (Md. Mahbub Alam).

0889-9746/$ - see front matter © 2007 Elsevier Ltd. All rights reserved.
doi:10.1016/j.jfluidstructs.2007.10.001

stagnant; (ii) the reattachment regime, where the shear layers separated from the upstream cylinder reattach on the downstream cylinder and the flow in the gap is still insignificant; (iii) the co-shedding regime, where the shear layers roll up alternately in the gap between the cylinders and thus the flow in the gap is significant. Zhou and Yiu (2006) and Xu and Zhou (2004) unearthed two distinct flow structures in the reattachment regime, depending on whether the shear layers from the upstream cylinder reattach on the downstream or upstream side of the downstream cylinder.

It is now well established that, in the co-shedding regime, the two circular cylinders shed vortices separately at the same frequency (Ishigai et al., 1972; Meneghini et al., 2001; Igarashi, 1984; Alam et al., 2003a, 2006; Xu and Zhou, 2004; Alam and Zhou, 2007a). Alam and Sakamoto (2005) used a square cylinder of the same characteristic height to replace the upstream cylinder, causing the vortex shedding frequency to be reduced, or to replace the downstream cylinder, which resulted in an increase in the shedding frequency. They have found in the co-shedding regime that, for a given downstream cylinder, different upstream-cylinder cross-sections with the same characteristic width resulted in a difference in the frequency of vortex shedding from the upstream cylinder, and the frequency of vortex shedding from the downstream cylinder adjusted itself to that of the upstream one. On the other hand, for a given upstream cylinder, a change in the downstream-cylinder cross-section produced no difference in its shedding frequency [see Alam and Sakamoto (2005) Alam and Zhou (2007a) for details]. It was concluded that the hydrodynamic stability of the flow around two tandem two cylinders is predominantly controlled by the upstream cylinder, not the downstream cylinder. The observation raises a number of questions. Firstly, would the two vortex shedding frequencies remain identical if the upstream cylinder diameter is changed, which will lead to a change in the vortex strength and frequency? Secondly, if the answer to the first question is yes, up to what diameter ratio? How does the Strouhal number depend on the ratio of the cylinder diameters? Thirdly, how would the flow downstream of the cylinders evolve, as compared with a single cylinder wake or the wake of two tandem cylinders of the same diameter? Finally, how would the fluid forces on the cylinders vary, as compared with those on an isolated cylinder or two tandem cylinders of the same diameter? It has been previously reported that placing a small cylinder upstream of a large cylinder, with their centre-to-centre spacing in the reattachment regime, could reduce significantly both time-averaged and fluctuating forces on the downstream large cylinder (Strykowski and Sreenivasan, 1990; Sakamoto et al., 1997; Lee et al., 2004). However, there is little information in the literature on the effect of a small cylinder on the forces on a large downstream cylinder with their centre-to-centre spacing in the co-shedding regime. These issues are both fundamentally and practically interesting and motivate the present investigation.

This work aims to study experimentally aerodynamic interference between two tandem circular cylinders of different diameters. The upstream cylinder diameter (d) is varied, with the downstream cylinder diameter (D) unchanged, so that the ratio d/D varies from 1.0 to 0.24. The flow structure, Strouhal number, time-averaged and fluctuating forces on the downstream cylinder are systematically measured.

2. Experimental details

Measurements were conducted in a low-speed, open-circuit wind tunnel with a 2.0 m long test-section of 0.35 m × 0.35 m. The flow in the test-section was uniform and the turbulent intensity was 0.5% at a free-stream velocity $U_\infty = 14$ m/s. Two brass cylinders were mounted in tandem in the vertical mid-plane of the working section. Fig. 1(a) shows schematically the experimental set-up and the definitions of coordinates (x', y') and (x, y), with the origins defined at the upstream and downstream cylinder centres, respectively. The upstream cylinder of diameter d was fixed-mounted at both ends, 0.2 m downstream from the exit plane of the contraction. The downstream cylinder of diameter D was cantilever-mounted, its lower end having a clearance of about 2–3 mm from the bottom wall of the working section (Fig. 1(b)). No vibration of the cylinder was observed. The diameter D was 25 mm and d was 25, 20, 15, 10 and 6 mm, respectively, and the corresponding d/D was 1.0–0.24, resulting in a maximum blockage of about 7.1%, and a minimum aspect ratio of 14. No end-plate was mounted. No vibration was observed even for the cylinder of the smallest diameter (6 mm). The upstream cylinder was fixed-supported at both ends through the same diameter hole of 30 mm long on the wind-tunnel walls. The vibration of a cylinder, fix-supported at both ends, in cross-flow may should be appreciable only when the vortex shedding frequency synchronized with the natural frequency of the fluid-cylinder system, which has been carefully avoided in the present experiments. The measurement were conducted at $U_\infty = 14$ m/s, corresponding to a Reynolds numbers (Re) of 2.72×10^4 and 0.65×10^4 based on the large and small cylinder diameters, respectively.

Two tungsten wires of 5 μm in diameter and approximately 2 mm in length, one (FH) fixed and placed at $x'/d = 2$, $y'/d = -1$ and the other (TH) traversed over $x/D = 1$–22, $y/D = 0.2$–4.0, were used to measure the frequencies of vortex shedding from the upstream and downstream cylinders, respectively (Fig. 1). The wires were operated at an overheat

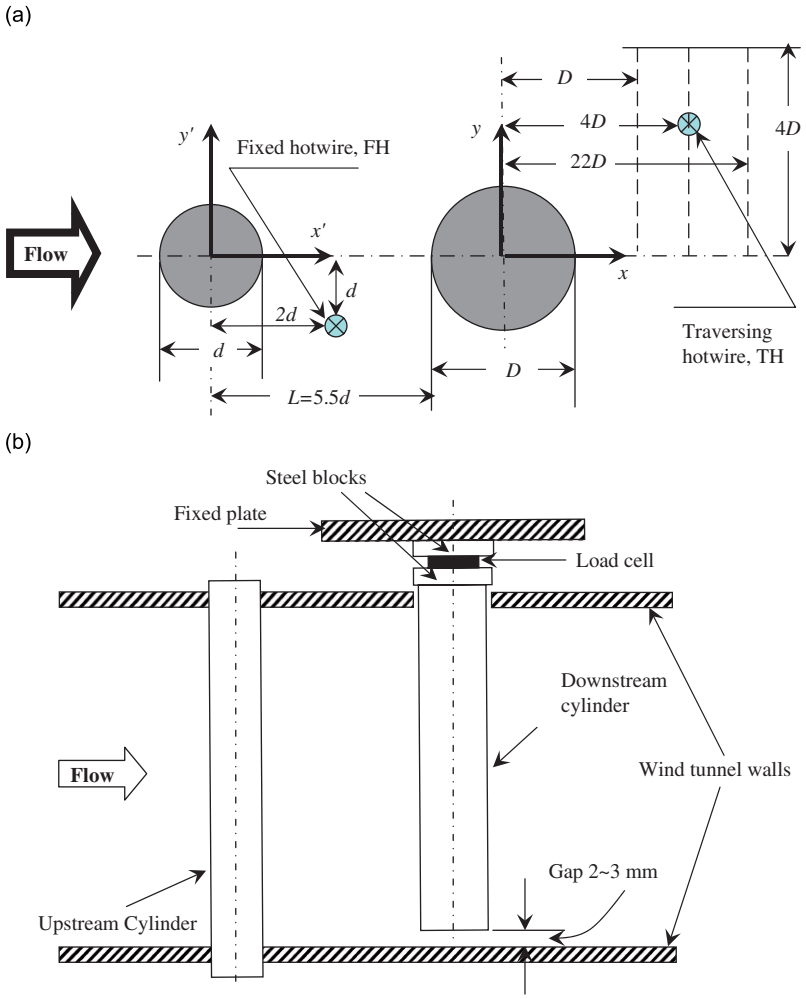

Fig. 1. (a) Schematic arrangement of experimental set-up. (b) Force measurement set-up.

ratio of 1.8 on a constant temperature circuit. The hot-wire probe holder was placed perpendicular to the wake-centre plane to minimize the disturbance to flow. It is known that, at a higher subcritical Re (2×10^3–10^5), vortices behind a single isolated cylinder roll up at $x'/d = 1.2$–2.0 and $y'/d = -0.7$ to -0.5 (Zdravkovich, 1997). The present Re based on the upstream cylinder is 6.5×10^3–2.72×10^4. Noting that the present experiment was conducted at $L/d = 5.5$, where the flow over the upstream cylinder was almost the same as that over an isolated single cylinder, the hot-wire should not affect the rollup of vortices, and its effect on the shear layer should be negligibly small. The signals from the wires were offset, amplified and then digitized using a 12-bit A/D board at a sampling frequency of 2.0 kHz. The sampling duration was about 16.2 s and at least three sample signals in one test were obtained at each measurement location. A signal exceeding 150 vortex shedding cycles in length may be considered to be stationary in the wake of a cylinder (Sakamoto et al., 1987). The presently measured minimum vortex shedding frequency was 67 Hz; a duration of 16.2 s corresponds to 1085 cycles, about 7.2 times the critical signal length. The power spectral density function, E_u, of the signals, calculated using a fast Fourier transform algorithm, was determined based on the average of 15 runs, each composed of 2048 (2^{11}) samples. Only repeatable dominant frequencies in the power spectrum were considered to be the dominant vortex frequencies. The frequency resolution in the power spectra was about 0.4 Hz.

A three-component quartz piezoelectric load cell (Kistler Model 9251A), characterized by high response, resolution and stiffness, was installed at the upper end of the downstream cylinder to measure the fluid forces. This load cell was bolted tightly between two machine-polished stainless steel blocks (Fig. 1(b)). In order to avoid the effect of wind tunnel vibration on the measurements, the holder of the load cell was mounted on an external rigid frame detached from the

wind tunnel. The load cell measures instantaneous integral fluid forces acting on the length of the cylinder exposed in the wind tunnel. The preload of the load cell was 25 kN, more than 7.4×10^4 times higher than the fluid forces presently measured, resulting in a very high signal-to-noise ratio.

A Dantec particle imaging velocimetry (PIV) was used to measure the near wake in the (x, y) plane. The cylinder surface and the tunnel working section wall hit by the laser sheet were painted black to minimize reflection noises. The flow was seeded by smoke, generated from Paraffin oil, with a particle size of about 1 μm in diameter. This measurement was conducted in a different wind tunnel, whose test-section was 0.6 m × 0.6 m and 2.4 m long. The velocity in the test-section was uniform to within 1% and the turbulent intensity was 0.7% at $U_\infty = 14$ m/s. See Huang et al. (2006), Alam and Zhou (2007b) for more details of the tunnel and the PIV system). The two cylinders have the same diameter as those used for the frequency and force measurements.

A two-component laser Doppler anemometry (LDA; Dantec Model 58N40 with enhanced FVA signal processor) was used to measure the cross-flow distributions of time-averaged and root mean square (rms) velocities at $x/D = -1.0$, 1.0 and 4.0. The LDA system was mounted on a three-dimensional (3-D) computer-controlled traversing mechanism, with a traversing resolution of 1 μm. This measurement was conducted in the wind tunnel with the 2.4 m long test-section of 0.6 m × 0.6 m.

The hot-wire and PIV/LDA measurements were carried out in two different wind tunnels of different working section dimensions. However, the cylinder diameters used were identical. Therefore, the minimum aspect ratio of the cylinders, corresponding to the large diameter cylinder used, was 14 and 24 in the hot-wire-measurement wind tunnel and PIV/LDA-measurement wind tunnel, respectively. West and Apelt (1993) established that the 'long' cylinder conditions, at which flow is independent of the cylinder spanwise length, prevail given a cylinder aspect ratio greater than 10. The aspect ratios of presently used cylinders all exceed the critical value for the 'long' cylinder condition. It may be inferred that the aspect ratios effect on results is negligibly small.

Flow visualization was conducted using the laser-induced fluorescence (LIF) technique in a water tunnel with a 0.5 m long working section of 0.15 m × 0.15 m. The upstream cylinder diameter was 15, 12, 9, 6 and 4 mm, and the downstream one was 15 mm, resulting in the same ratios of diameters as used in the wind tunnels. Both cylinders were made of acrylic, and L/d was 5.5. The Reynolds numbers were 450 and 180 based on the large and small diameters, respectively. Dye (Rhodamine 6G 99%) was introduced into the flow through two pin holes at the mid-span of the two cylinders and 90° clockwise and anti-clockwise, respectively, from the leading stagnation point. A thin laser sheet, generated by laser beam sweeping, provided illumination in the vertical plane through the mid-span of the cylinders. A Spectra-Physics Stabilite 2017 Argon Ion laser (4 W) was used to generate the laser beam. A digital video camera was used to record the dye-marked vortex street at a framing rate of 25 frames per second. The camera view window was set first at $x'/d = -1$–$x/D = 3$ and then at $x/D = -1.0$–13. The duration of each recording was 10 min.

3. Wavelet and cross-wavelet analyses

The Fourier transform produces averaged spectral coefficients that are independent of time and is useful to identify dominant frequencies in a signal. When a Fourier spectrum from the signal displays more than one peak, the information on the frequencies, at which the peaks occur, with respect to time, i.e., frequency-time plots, is very valuable to the understanding of flow physics (Farge, 1992; Alam et al., 2003b; Alam and Sakamoto, 2005). This information may be given in the short term Fourier transform (STFT). However, STFT may suffer from limitations (Daubechies, 1990; Newland, 1993; Hamdan et al., 1996; Torrence and Compo, 1998). The limitations may be avoided if the wavelet transform is deployed, which produces a potentially more revealing picture of the time–frequency localization of signals. Although relatively new, wavelet analysis has found many applications in fluid mechanics, for example, to identify predominant frequencies in a coaxial jet flow (Li, 1997; Yilmaz and Kodal, 2000), to explicate fundamental vibration frequencies of a self-excited cylinder (Hamdan et al., 1996), to study the turbulent structures of different scales in a turbulent cylinder wake (Rinoshika and Zhou, 2005a, b). Recently, Alam and Sakamoto (2005) and Alam et al. (2003b) used wavelet and cross-wavelet transforms to characterize the switching phenomena of the gap flow between two circular cylinders in staggered, tandem and side-by-side arrangements. Alam et al. (2003b) observed, based on the wavelet analysis of two simultaneously obtained hot-wire signals measured in a two-side-by-side-cylinder wake, how the vortex frequency associated with one cylinder changed at the bi-stable flow regime with respect to that associated with the other and with respect to time. They managed to identify, based on cross-wavelet analysis, the synchronized frequency, the synchronized region in time space, and phase between the processes of vortex shedding from the two cylinders.

The wavelet transform is a linear convolution (Yong, 1998) of a given one-dimensional signal $u(t)$ and the mother wavelet $\psi(t)$. Mathematically, the wavelet transform is given by

$$W(s,b) = \frac{1}{\sqrt{s}} \int u(t) \Psi^{\#} \left(\frac{t-b}{s} \right) \mathrm{d}t, \tag{1}$$

where $W(s,b)$ is the wavelet coefficient, the superscript '#' denotes the complex conjugate, b is the translation parameter, and s is the scale parameter. $W(s,b)$ may be given graphically in the wavelet map in terms of s and b for a given mother wavelet. A large value of $W(s,b)$ reflects the combined effect of a large fluctuation of the signal and of good matching in the shape between the signal and the wavelet.

There are many mother wavelets used in practice, e.g., the Morlet wavelet, the Mexican hat wavelet, and the Gabor wavelet. The Mexican hat wavelet is real-valued, and the Morlet and Gabor wavelets are complex-valued. The real-valued wavelet isolates the local minima and maxima of a signal. When a complex-valued mother wavelet is used in Eq. (1), $W(s,b)$ becomes complex, with a real part, $W^R(s,b)$, and an imaginary part, $W^I(s,b)$. While $W^2(s,b) = W^{R^2}(s,b) + W^{I^2}(s,b)$ provides the information on the frequency domain of a signal, $W^R(s,b)$ is important to identify the minima and maxima of a signal with regard to frequency (Farge, 1992). The choice of appropriate mother wavelet depends on the information we need to extract from the signal (Rinoshika and Zhou, 2005b). For example, information extracted using the Mexican hat wavelet is highly localized in the time domain and poorly localized in the frequency domain. The Gabor wavelet has a good frequency resolution but a poor time resolution, compared with the Mexican hat; its frequency resolution is however poorer, although its time resolution is better, than the Morlet wavelet. The Morlet wavelet is used herein and is expressed as:

$$\Psi(t) = \pi^{-1/4} \, \mathrm{e}^{\mathrm{i}\omega_0 t} \, \mathrm{e}^{-t^2/2}, \tag{2}$$

where ω_0 is the wave number in the Morlet wavelet, chosen to be 6.0 to satisfy the admissibility condition (Farge, 1992; Li, 1997). At this value of ω_0, the relation between scales, s, and Fourier frequencies is $f = 1/(1.03s)$ (Torrence and Compo, 1998). Given wavelet transforms $W_1(s,b)$ and $W_2(s,b)$ of two time series, the cross-wavelet spectrum $W_{12}(s,b)$ is defined by

$$W_{12}(s,b) = W_1(s,b) W_2^{\#}(s,b), \tag{3}$$

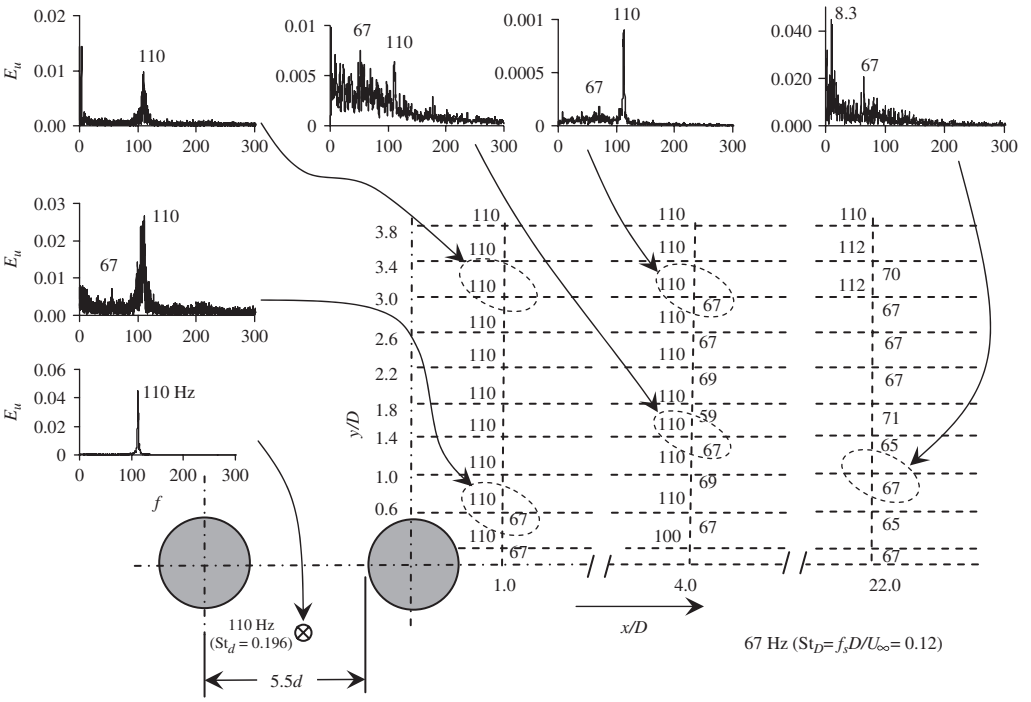

Fig. 2. The power spectral density function of hot-wire signals for $d/D = 1.0$ ($d = 25$ mm, $D = 25$ mm).

where $W_2^{\#}(s,b)$ is the complex conjugate of $W_2(s,b)$. If the analysis is carried out based on a complex wavelet, as with the Morlet wavelet used herein, the cross-wavelet spectrum $W_{12}(s,b)$ is also complex, and hence $W_{12}(s,b)$ consists of real and imaginary parts, i.e., $W_{12}^R(s,b)$ and $W_{12}^I(s,b)$. The cross-wavelet $W_{12}(s,b)$ reflects the similarity (coherence) between the signals in terms of both frequency and localization (in time space). More details of wavelet and cross-wavelet analysis could be found in Torrence and Compo (1998) and Alam et al. (2003c).

4. Results and discussion

4.1. Vortex shedding frequency

Fig. 2 presents the typical power spectral density functions (E_u) of the measured hot-wire signals for $d/D = 1.0$. A table is inserted in the figure to list frequencies at which the pronounced peaks in E_u occur. A single pronounced peak occurs at 110 Hz in E_u of signal u, measured in the gap of the two cylinders, indicating the frequency, f_s, of vortex

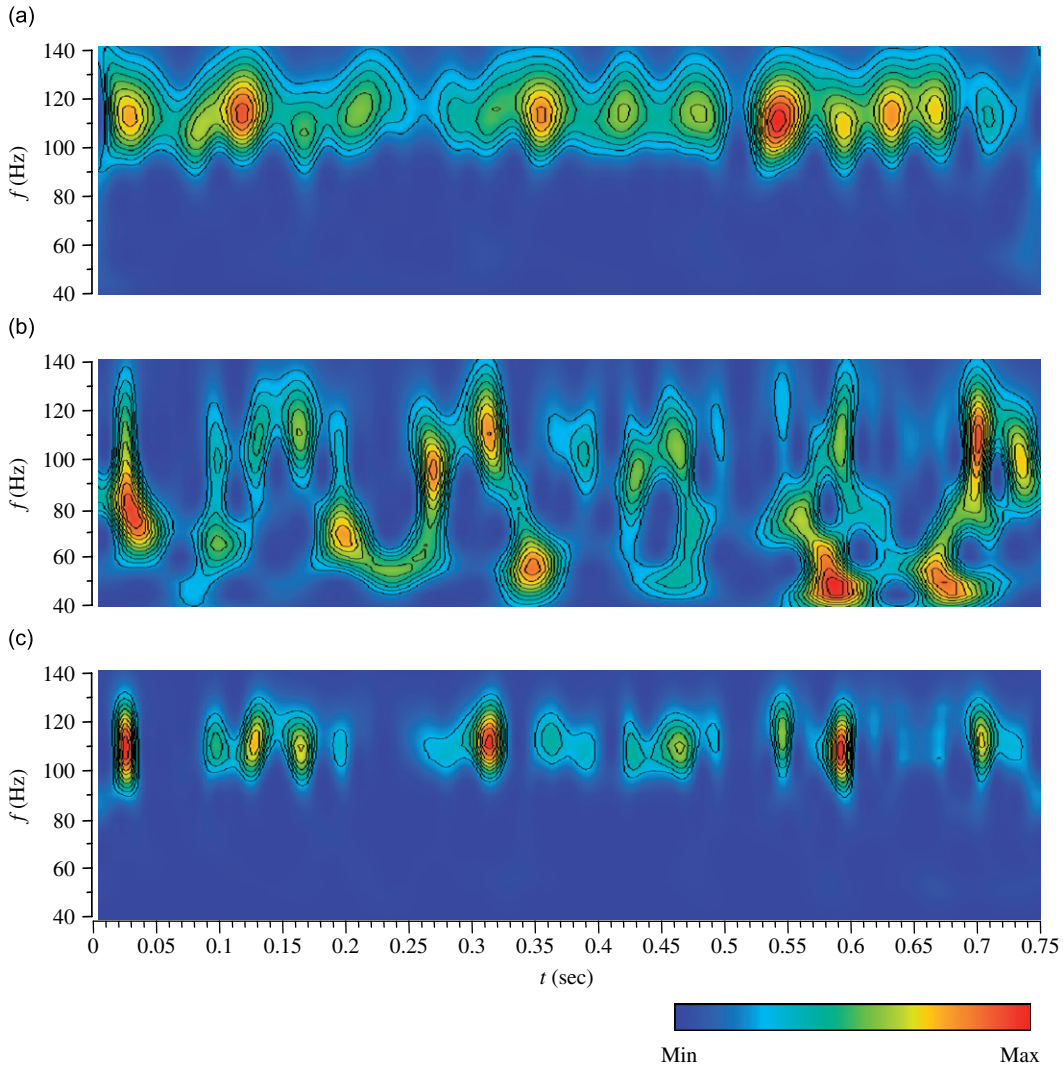

Fig. 3. Wavelet scalogram of hot-wire signals ($d/D = 1.0$): (a) between cylinders, (b) behind cylinders ($x/D = 4$, $y/D = 1.4$), and (c) cross-wavelet scalogram of the two hot-wire signals. The outer contour enclosed 80% of maximum energy.

shedding from the upstream cylinder. The corresponding Strouhal number, St_d ($=f_s d/U_\infty$), is 0.196, approximately equal to the presently measured value (0.198) behind an isolated cylinder. However, two peaks are identifiable in E_u behind the cylinders. The one at $f=110$ Hz is rather pronounced and is the same as measured between the cylinders, and the other occurs at 67 Hz or $St_D=f_s D/U_\infty=0.12$. The peak at $St_d=0.196$ is detected across the wake, over $y/d=0$–3.8, from $x/D=1$ to 4, but is identifiable only for $y/d=3$–3.8 at $x/D=22$. The observation is consistent with previous reports at similar Re and L/d (Xu and Zhou, 2004; Zhou and Yiu, 2006). The peak at $St=0.12$ is barely identifiable, which is probably why this St value has been overlooked in previous measurements (Igarashi, 1984; Kiya et al., 1980; Xu and Zhou, 2004; Zhou and Yiu, 2006). At a close vicinity of the downstream cylinder, this peak is detectable only within the central region of the wake, e.g., at $y/d<0.6$ at $x/D=1$. This detectable region grows laterally downstream, up to $y/d=3.0$ at $x/D=4$ and $y/d=3.4$ at $x/D=22$. Furthermore, this peak becomes weaker with increasing y/D. The observation suggests that vortex shedding from the downstream cylinder be responsible for the peak at $St_D=0.12$. The peak at 67 and 110 Hz becomes stronger and weaker, respectively, with increasing x/D, implying that, while the vortices of 110 Hz decay downstream, those of 67 Hz grows. The power spectrum displays a peak at 8.3 Hz at $x/D=22$ and $y/D=1.0$, which is probably caused by a low frequency noise.

Ishigai et al. (1972) and Igarashi (1984) reported a bi-stable flow phenomenon, that is, the stable reattachment and co-shedding occur intermittently at the same L/d and Re. Xu and Zhou (2004) found a different bi-stable flow phenomenon, where two stable flow states, i.e., the shear layer rollup behind and reattachment on the downstream cylinder, may co-exist at the same L/d ($=2$–3) and Re, though not necessarily in time. Both bi-stable phenomena are associated with the simultaneous occurrence of two distinct Strouhal numbers. The present observation differs from the bi-stable phenomena. Due to a disparity in incident flow conditions, the shear layers around the upstream cylinder should be associated with different instability frequencies compared to those around the downstream cylinder, thus resulting in two distinct Strouhal numbers observed behind the downstream cylinder.

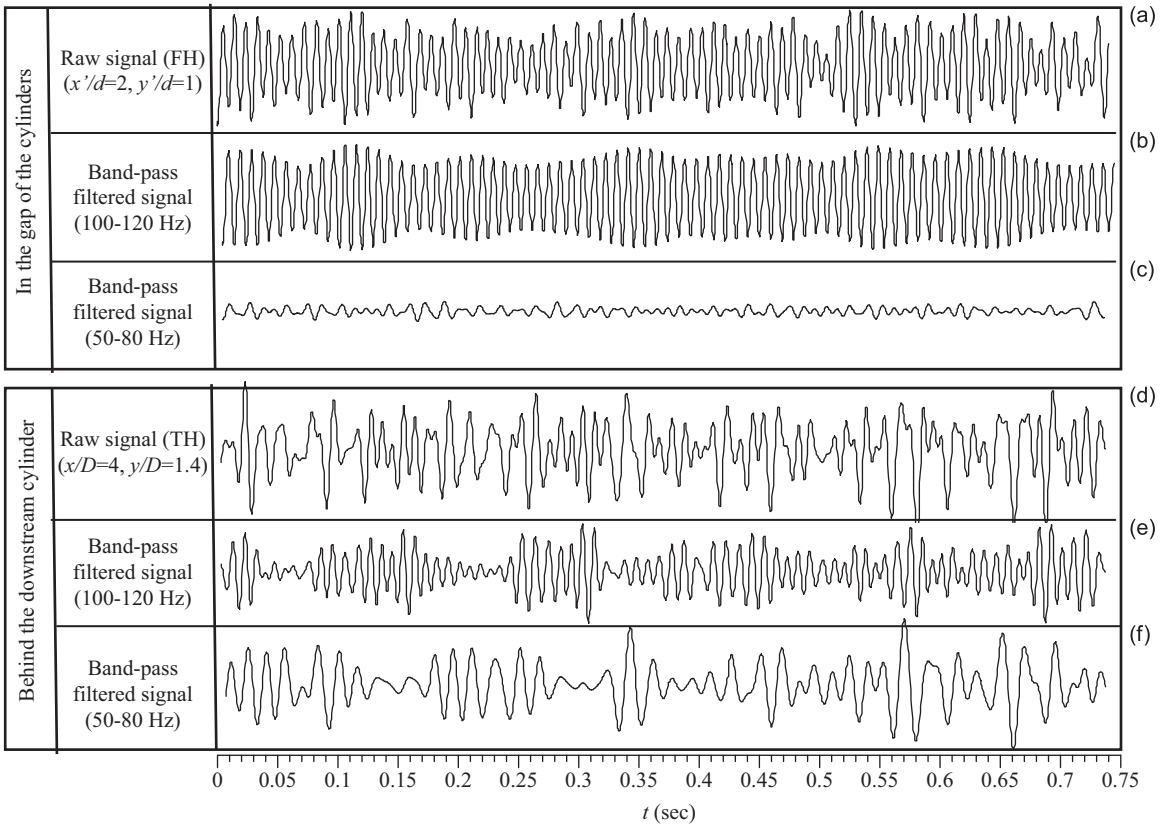

Fig. 4. Hot-wire signals ($d/D=1.0$) and their band-pass filtered signals. The ordinate of the FH raw signal and its band-pass filtered signals are scaled from −0.4 to 0.4 V and that of the TH raw signal and its band-pass filtered signals are −0.75 to +0.75 V.

The occurrence of the peak at $St_d = 0.196$ behind the cylinders may be ascribed to two different scenarios: (i) the advection and/or impingement of vortices shed from the upstream cylinder; (ii) an intermittent lock-in of vortex shedding from the downstream cylinder to vortices adveceted from the upstream cylinder. Fig. 3 shows the wavelet and cross-wavelet analysis results of FH and TH signals measured simultaneously between and behind the cylinders, respectively. A close examination of the figure unveils that vortex shedding from the upstream cylinder occurs at a frequency of 110 Hz (Fig. 3(a)), while that from the downstream is 110 Hz, e.g., at time $t = 0.12$–0.18 s and 0.26–0.33 s in Fig. 3(b) and 67 Hz, e.g., at $t = 0.02$–0.06 s and 0.18–0.26 s. The higher vortex frequency (110 Hz) appears in two modes, i.e., simultaneously with the lower vortex frequency (e.g. at $t = 0.02$–0.03 s, 0.08–0.1 s, 0.44–0.47 s, 0.58–0.6 s) and in the absence of the lower vortex frequency (e.g. at $t = 0.12$–0.18 s, 0.26–0.33 s, 0.37–0.38 s). In the first mode, vortex shedding from the downstream cylinder occurs at 67 Hz and co-exists with the vortices of 110 Hz advected from the upstream cylinder; in the second mode, vortex shedding from the downstream cylinder is locked-in with the frequency of vortices originating from the upstream cylinder. The lock-in of the two shedding processes may be identified unequivocally from the cross-wavelet (Fig. 3(c)) in terms of the lock-in instant, duration and intermittency. Apparently, the lock-in occurs at a frequecny of 110 Hz and at a time t when the wavelet scalogram is concentrated, e.g., at $t = 0.12$–0.18 s and 0.26–0.33 s.

The above observation could also be extracted from the digitally band-pass filtered signals of the fluctuating velocity between and behind the cylinders (Fig. 4). As two dominant frequencies were detected at 67 and 110 Hz behind the downstream cylinder, the TH signal at $x/D = 4$ and $y/D = 1.4$ was band-pass filtered with a band of 50–80 Hz and 100–120 Hz, respectively, in order to extract information in the signals around the central frequencies of 67 and 110 Hz, respectively (Fig. 4(d–f)). The FH signal is also filtered at the same band-pass frequencies (Fig. 4(a–c)). Both raw and filtered FH signal fail to show the presence of the frequecny component of 67 Hz in the gap of the cylinders. On the other hand, both raw and filtered TH signals contain the two frequency components of 67 and 110 Hz, suggesting that vortices may switch from one frequency to the other, or may occur simultatneously at both high and low frequencies, as observed in the wavelet analysis results. For example, the TH signal exhibits the frequecny of 110 Hz at $t = 0$–0.02 s (Fig. 4(e)), and the frequencies of both 67 and 110 Hz at $t = 0.02$–0.03 s (Fig. 4(e, f)) and only the frequecny of 67 Hz at

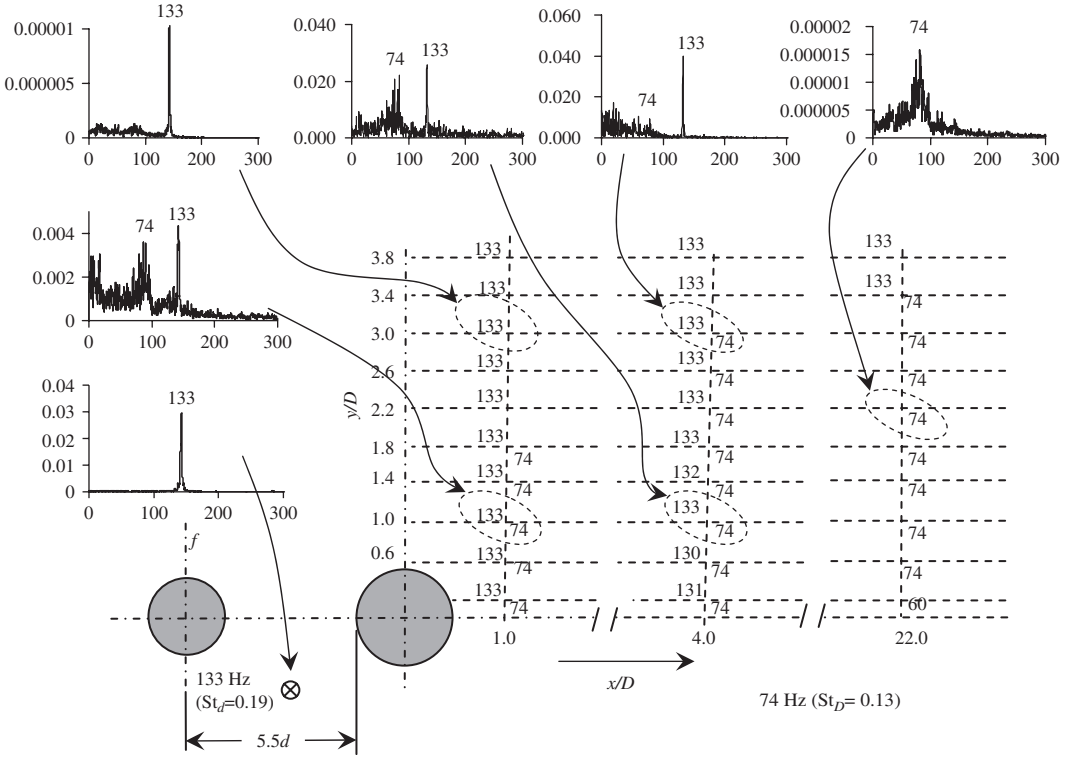

Fig. 5. The power spectral density function of hot-wire signals for $d/D = 0.8$ ($d = 20$ mm, $D = 25$ mm).

$t = 0.03$–0.08 s (Fig. 4(f)), then again both at $t = 0.08$–0.1 s (Fig. 4(e, f)), and then returns to the frequecny of 110 Hz at $t = 0.11$–0.18 s (Fig. 4(e)).

In their investigation of the lateral vibrations of two tandem cylinders ($L/D = 6.5$) of the same diameter in a free surface water channel, King and Johnes (1976) obserevd two peaks in the dependence of the measured vibraion amlitude of the downstream cylinder on the reduced velocity U_r ($= U_\infty/nD$, where n is the structural natural frequecny of the cylinders), one at $U_r = 5.5$ and the other at $U_r = 7.5$. The one at $U_r = 5.5$ ($\mathrm{St} = 1/U_r = 0.182$) resulted from the excittation at the frequency of vortex shedding from the upstream cylinder. However, they could not explain the other peak at $U_r = 7.5$, which was more pronounced than that at $U_r = 5.5$. Since $U_r = 7.5$ corresponds to $\mathrm{St} = 0.13$, the frequencies, at which their observed peaks occurred, agree well with the presently measured $\mathrm{St}_d = 0.196$ and $\mathrm{St}_D = 0.12$, respectively. We may offer one explanation from the present findings, that is, their peak at $U_r = 7.5$ resulted from the excitation of vortex shedding from the downstream cylinder.

Fig. 5 presents E_u for $d/D = 0.8$. The frequencies of vortex shedding from the upstream and downstream cylinders are 133 Hz or $\mathrm{St}_d = 0.19$ and 74 Hz or $\mathrm{St}_D = 0.13$, respectively. The peak at 74 Hz in E_u measured behind the downstream cylinder is more significant than that for $d/D = 1.0$, and is discernible up to $y/D = 1.8$ at $x/D = 1.0$. The cross-wavelet scalogram displays concentrations around 133 Hz, e.g., at $t = 0.11$–0.15 s, 0.33–0.35 s, 0.54–0.57 s in Fig. 6(c), indicating the intermittent lock-in of vortex shedding from the downstream cylinder with that from the upstream. The wavelet scalogram of the signals measured behind the downstream cylinder shows from time to time concentrations

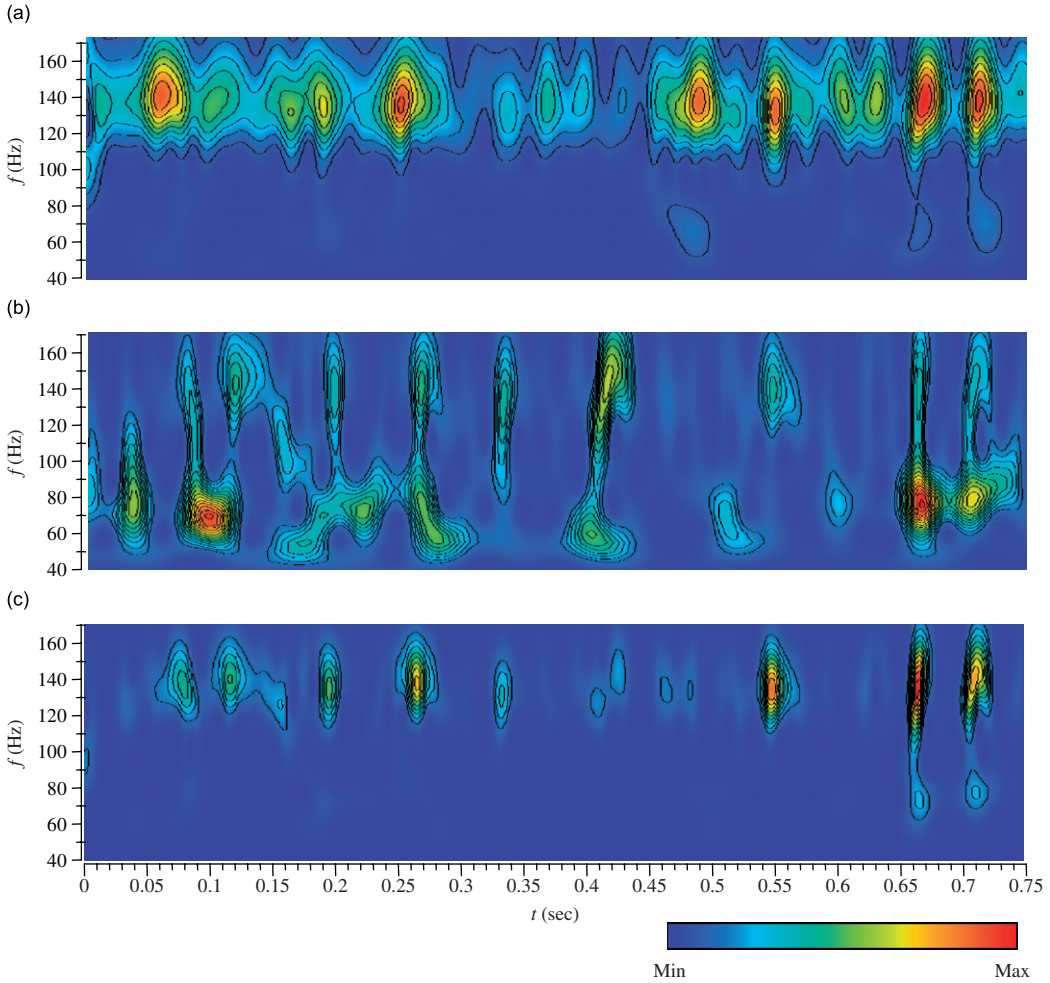

Fig. 6. Wavelet scalogram of hot-wire signals at $d/D = 0.8$: (a) between cylinders, (b) behind cylinders ($x/D = 4$, $y/D = 1.0$), and (c) cross-wavelet scalogram of the two hot-wire signals. The outer contour line enclosed 80% of maximum energy.

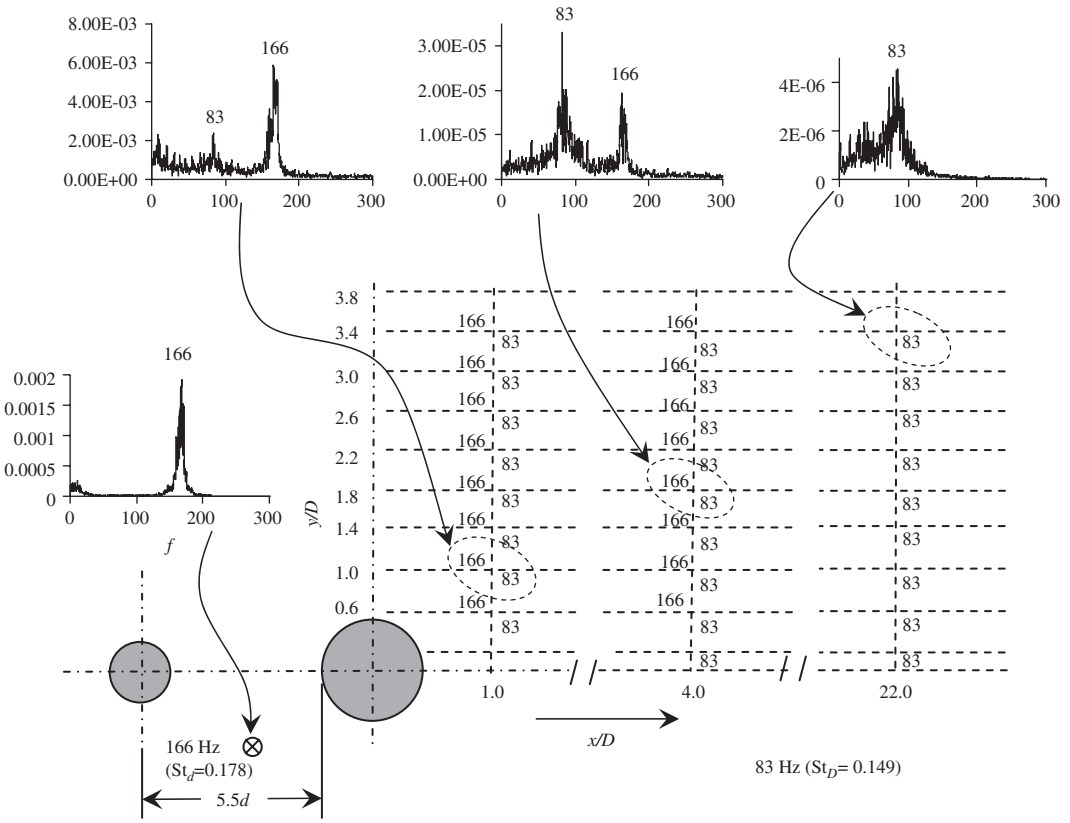

Fig. 7. The power spectral density function of hot-wire signals for $d/D = 0.6$ ($d = 15$ mm, $D = 25$ mm).

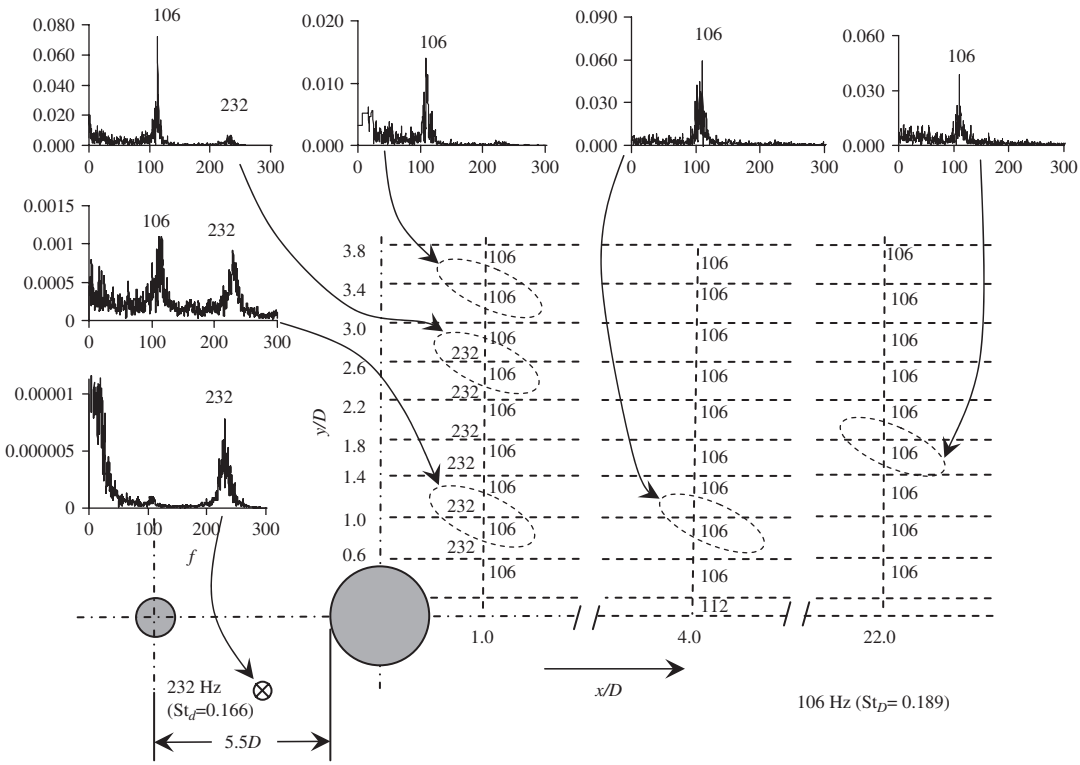

Fig. 8. The power spectral density function of hot-wire signals for $d/D = 0.4$ ($d = 10$ mm, $D = 25$ mm).

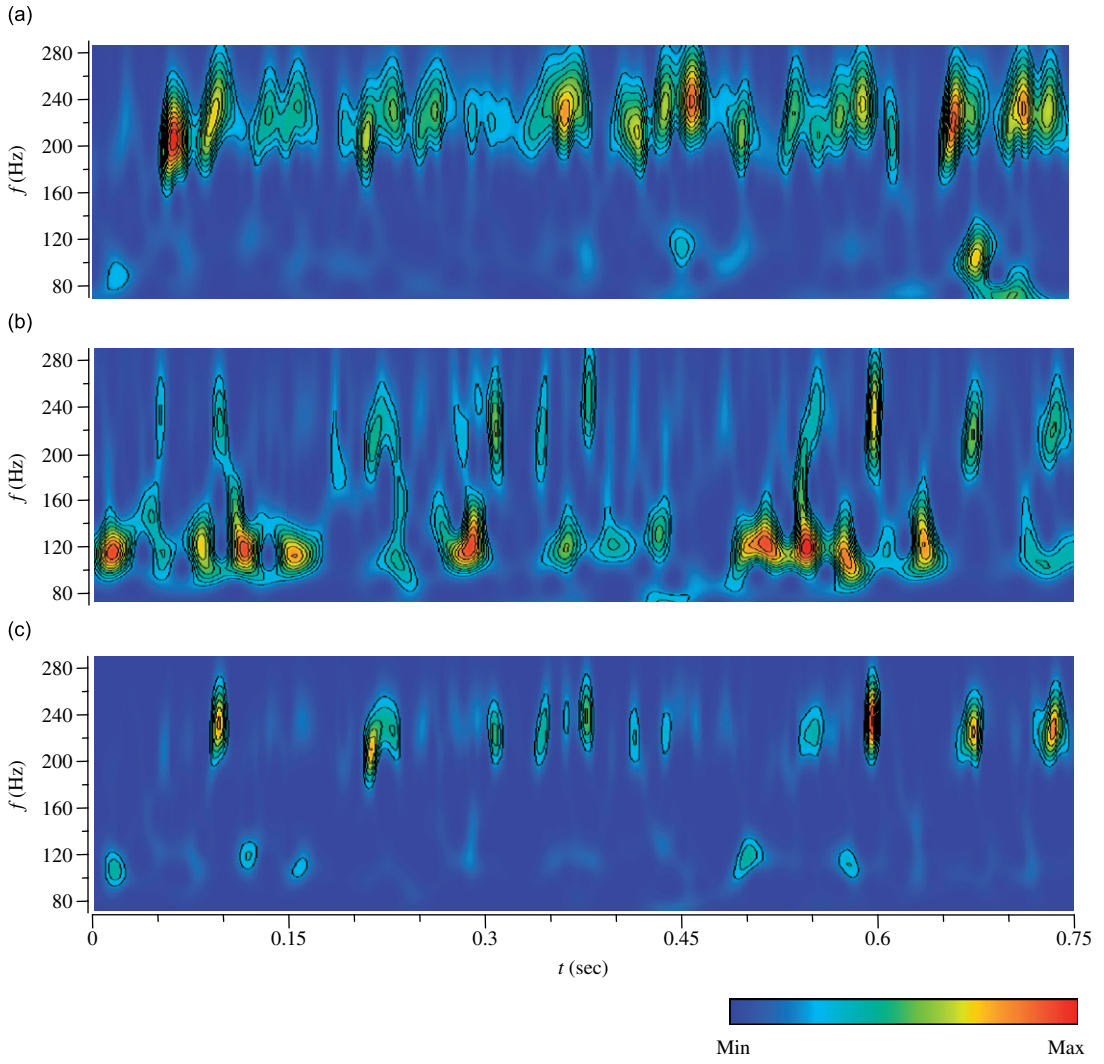

Fig. 9. Wavelet scalogram of hot-wire signals at $d/D = 0.4$: (a) between cylinders, (b) behind cylinders ($x/D = 1$, $y/D = 1$), and (c) cross-wavelet scalogram of the two hot-wire signals. The outer contour line enclosed 80% of maximum energy.

simultaneously around 133 and 74 Hz, e.g., at $t = 0.09$–0.1 s, 0.2–0.21 s, 0.27–0.29 s in Fig. 6(b). Similar observations are made for $d/D = 0.6$ (Fig. 7) and 0.4 (Fig. 8). For $d/D = 0.6$, the peak at 166 Hz is more pronounced at $x/D = 1$ than at 83 Hz, but becomes weaker at $x/D = 4$. By $x/D = 22$, the peak at 166 Hz vanishes completely. For $d/D = 0.4$, the low-frequency peak overwhelms the high-frequency peak even at $x/D = 1$, the latter being discernible only at $y/D = 0.6$–2.6. In fact, the high frequency peak cannot be observed at $x/D \geqslant 4$. The wavelet and cross-wavelet scalograms at $d/D = 0.4$ (Fig. 9) shows that the vortex shedding from the downstream cylinder is intermittently locked-in with the vortices originating from the upstream cylinder; however, the lock-in duration shrinks considerably, compared with larger d/D.

As d/D drops to 0.24 (Fig. 10), two pronounced peaks were observed at 404 Hz or $St_d = 0.173$ and 114 Hz or $St_D = 0.203$ in the gap of the two cylinders. The former originates from vortex shedding from the upstream cylinder and is absent behind the downstream cylinder, except a tiny hump at $x/D = 1$ and $y/D = 1$–1.8 (see E_u at $y/D = 1.4$ and $x/D = 1$). The latter occurs at $x/D > 0$, apparently resulting from vortex shedding from the downstream cylinder. Being very small compared with the downstream cylinder, the upstream cylinder produces very weak vortices, which fail to lock in vortex shedding from the downstream cylinder. Interestingly, the hot-wire in the gap of the cylinders captures quite convincingly the information on vortex shedding from the downstream cylinder, suggesting that alternate vortex

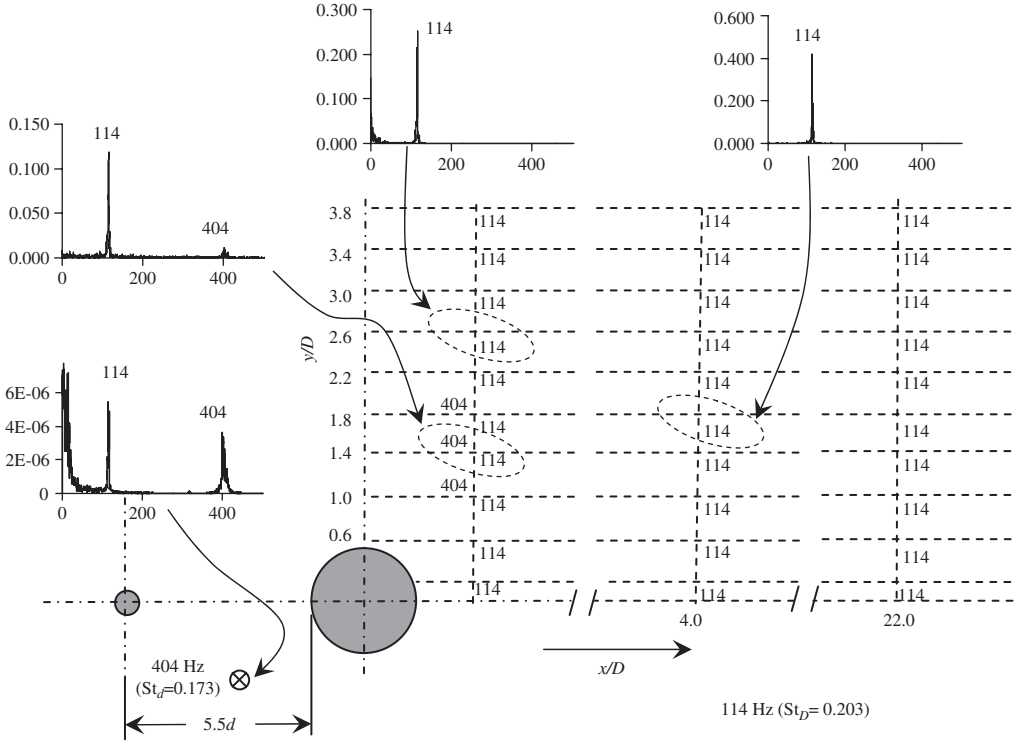

Fig. 10. The power spectral density function of hot-wire signals for $d/D = 0.24$ ($d = 6$ mm, $D = 25$ mm).

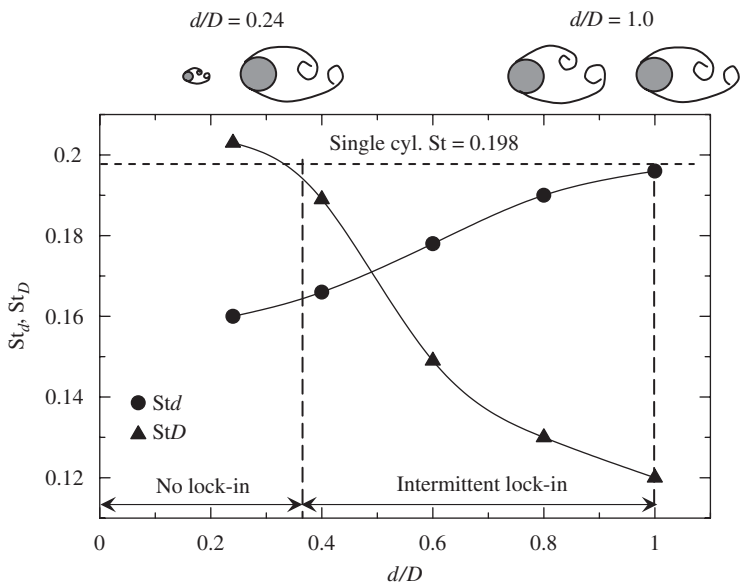

Fig. 11. Dependence of Strouhal numbers on d/D.

shedding from the downstream cylinder feeds back upstream rather strongly, well exceeding the influence of vortices advected from the upstream cylinder. As a matter of fact, this upstream feedback is also discernible at $d/D = 0.4$, where a faint peak occurs in E_u measured in the gap of cylinders (Fig. 8), but not at a larger d/D.

In summary, the frequency of vortex shedding from the downstream cylinder is in general lower than that from the upstream cylinder. The two frequencies may be intermittently locked-in for $d/D = 0.4$–1.0, but not for $d/D < 0.4$. Behind

the cylinders, the y/D range where the high-frequency vortices are captured diminishes with declining d/D, because of weakened vortices from the upstream cylinder. Accordingly, the peak of the lower frequency grows in E_u, compared with that of the higher frequency. The observation is linked to an increasing incident flow velocity, at a smaller d/D, to the downstream cylinder.

Fig. 11 summarizes the dependence on d/D of St_d and St_D, associated with the upstream and downstream cylinders, respectively. The Strouhal number measured herein ($St = 0.198$) behind an isolated circular cylinder is also given. At $d/D = 1.0$, St_d is 0.196, very close to St. The value of St_d displays a variation opposite to that of St_D; St_d decreases for a smaller d/D. It is likely that the downstream cylinder acts to block the flow. This effect is more significant at small d/D, which may prolong the period of vortex shedding from the upstream cylinder, thus decreasing St_d. On the other hand, St_D increases with decreasing d/D. At $d/D = 1.0$, St_D is rather small, 0.12, because the approaching gap flow velocity at the downstream cylinder is significantly lower than that at the upstream cylinder or a single isolated cylinder. With decreasing d/D, the upstream cylinder wake becomes narrower and the flow velocity approaching the upstream side of the downstream cylinder increases (as will be discussed in Sections 4.2.1 and 4.2.2), resulting in an increase in St_D.

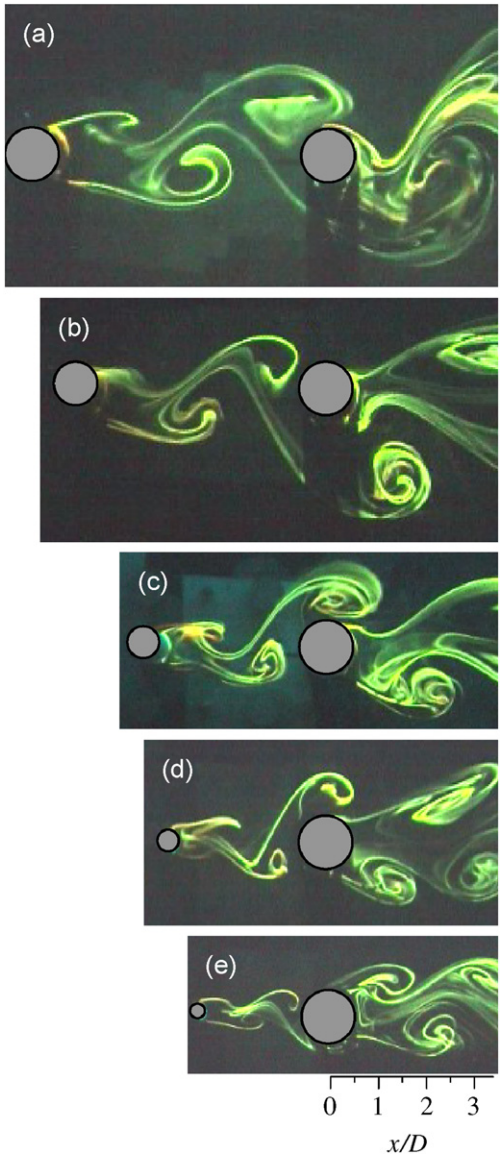

Fig. 12. Photographs of wake in the gap with change in d/D: (a) $d/D = 1$, (b) 0.8, (c) 0.6, (d) 0.4, and (e) 0.24.

4.2. Flow structure

4.2.1. Vortex street

Fig. 12 presents typical photographs from laser-induced fluorescence flow visualization of the flow between the cylinders at various d/D. With decreasing d/D, the upstream-cylinder wake narrows and the size of vortices appears smaller. However, the vortex street is qualitatively unchanged. The advected alternately arranged vortices impinge upon the downstream cylinder; and the impinging width across the downstream cylinder diminishes, with respect to the scale of the downstream cylinder wake, with decreasing d/D. The observation is consistent with the absence of the higher frequency peak in E_u at $y/D > 2.6$ ($x/D = 1$) for $d/D = 0.4$ (Fig. 8) and at $y/D > 1.8$ ($x/D = 1$) for $d/D = 0.24$ (Fig. 10). The alternating vortex impingement upon the downstream cylinder acts essentially as a quasi-periodic excitation, thus locking-in vortex shedding from the downstream cylinder given adequate strength. The present data demonstrate that vortex shedding from the downstream cylinder is almost completely locked-in with this excitation at $d/D = 1$, but only intermittently for $0.4 \leqslant d/D < 1$ because of the reduced strength of excitation. The excitation is too weak to lock in vortex shedding from the downstream cylinder at $d/D < 0.4$.

Two types of vortex shedding from the downstream cylinder were observed in flow visualization for $d/D = 0.4$–1.0, one coupled (locked-in) with vortex shedding from the upstream cylinder at the higher dominant frequency and the other decoupled at the lower dominant frequency. They switched frequently from one to the other, as observed in the hot-wire signals. Fig. 13 shows typical photographs taken behind the downstream cylinder ($d/D = 0.4$). By counting vortices shed from the cylinders within a given duration, the frequencies of coupled and decoupled vortex shedding from the downstream cylinder may be estimated. In the decoupled case (Fig. 13(a)), vortex shedding from the downstream cylinder was at a frequency lower than from the upstream cylinder, and the flow structure was characterized by an alternate vortex street. In the coupled case (Fig. 13(b)), a higher vortex frequency was detected in the very near wake. Note that the vortices at $x/D < 5$ appear at a higher frequency than further downstream, consistent with the hot-wire measurement (Section 4.1). When advected downstream, the high frequency vortices are unstable and reorganize themselves to the lower frequency, which is determined by the inherent instabilities of shear layers in the wake of the two tandem cylinders.

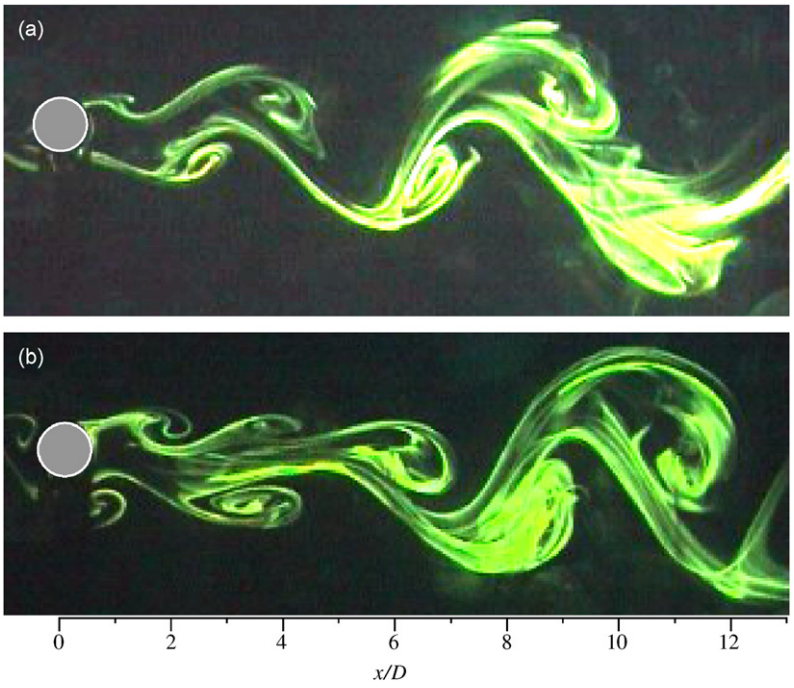

Fig. 13. Distinct flow structures captured at different instants behind the downstream cylinder, $d/D = 0.4$, $\mathrm{Re}_D = 450$. (a) Low-frequency vortices generated by the downstream cylinder, which are decoupled from those shed from the upstream cylinder. (b) High-frequency vortices generated by the downstream cylinder ($x/D < 5$), which are coupled with those originating from the upstream cylinder. Note the low-frequency vortices at $x/D > 5$.

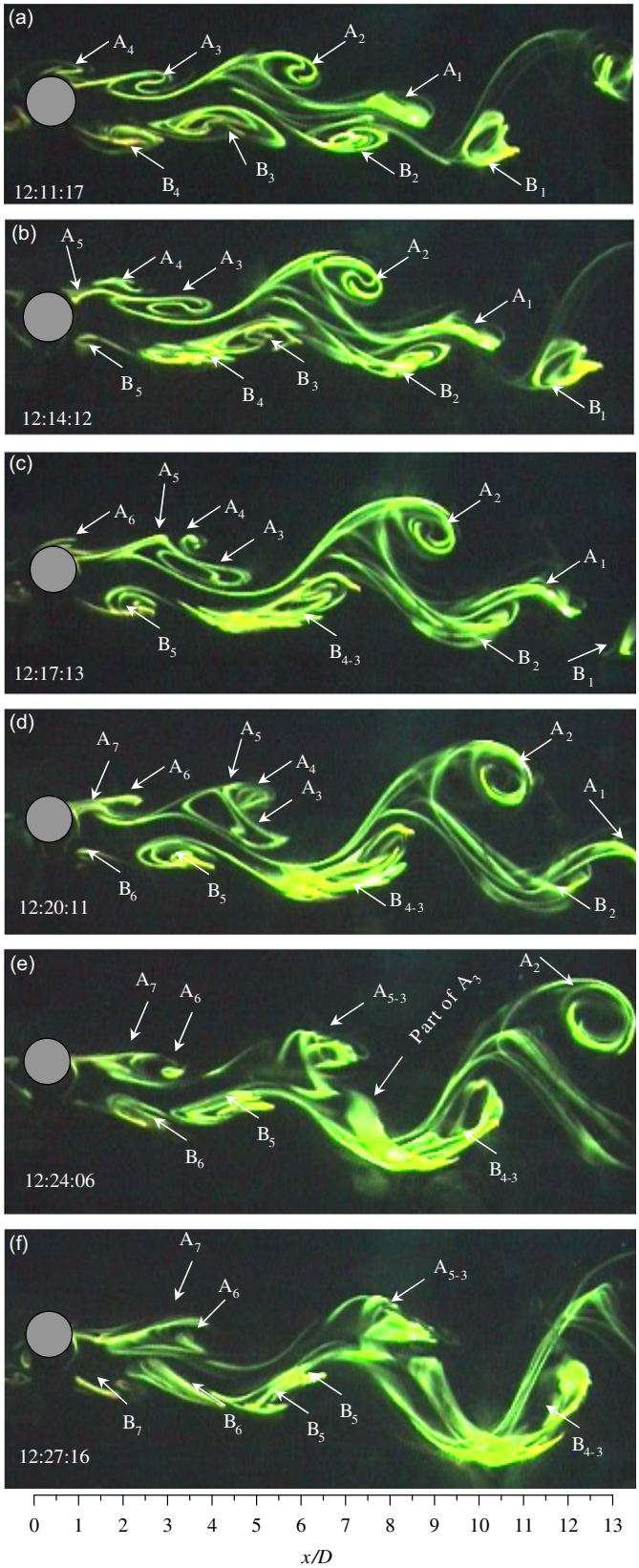

Fig. 14. Sequential photographs of the wake behind the downstream cylinder, illustrating the vortex evolution from high frequency to low frequency ($d/D = 0.4$).

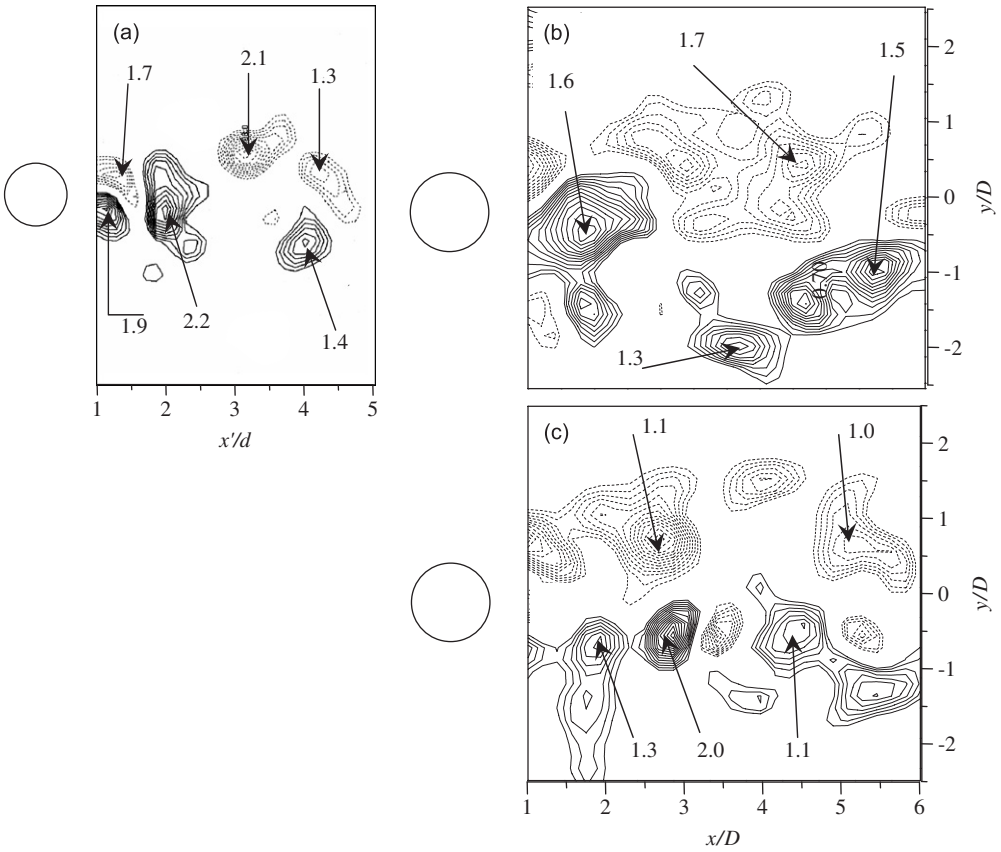

Fig. 15. Iso-contours of instantaneous vorticity at $d/D = 0.8$: (a) $\omega_z^* = \omega_z d/U_\infty$ between the cylinders; (b, c) $\omega_z^* = \omega_z d/U_\infty$ behind the cylinders, decoupled and coupled vortex shedding, respectively. Contour increment = 0.1. Cut-off level of $\omega_z^* = 0.35$.

It can be insightful to examine how vortices, when advected downstream, evolve from the high frequency observed in the near wake of the downstream cylinder to the low frequency. Fig. 14 presents sequential photographs ($Re_D = 450$) taken behind the downstream cylinder in order to explicate the evolution process. The three numbers of time index given at the lower left-hand side corner in each plate represent minute, second and frame number (the framing rate = 25 fps), respectively. The high-frequency vortices, as marked, are evident near the downstream cylinder in Fig. 14(a), where vortex A_4 is about to separate from the upper side of the cylinder. In the following plate (Fig. 14(b)), A_4 completes its separation in Fig. 14(b), and vortices B_3 and B_4 appear distorted and approach each other. Similarly, A_3 and A_4 on the other side of the wake approach each other and appear approached by the following A_5 (Fig. 14(c)). At the same time, B_4 and B_3 have completed their merging, forming a larger vortex B_{4-3}. The vigorous interactions among approaching vortices cause A_5, A_4 and A_3 to distort. Fig. 14(d) shows that A_5 and A_4 have amalgamated and pinched part of A_3, forming a larger vortex A_{5-3} (Fig. 14(e, f)). The other part of A_3 appears detached from A_{5-3} (Fig. 14(e)). Apparently, the processes of distortion, splitting and amalgamation eventually lead to the evolution of the high-frequency vortices to the low frequency, probably under the underlying inherent instability of the wake behind the downstream cylinder.

Fig. 15 presents typical instantaneous vorticity contours, $\omega_z^* = \omega_z D/U_\infty$, measured using PIV. The asterisk stands for normalization by D and/or U_∞. For the purpose of comparison, the cut-off level and increment of the contours are made the same for the plots. Again two distinct flow patterns are observed behind the downstream cylinder, one characterized by large-scale and low-frequency vortices (Fig. 15(b)) and the other by relatively small-scale vortices (Fig. 15(c)), whose frequency is the same as that of vortices generated by the upstream cylinder (Fig. 15(a)).

4.2.2. *Time-averaged and fluctuating velocities*

Figs. 16 and 17 present the time-averaged and root mean square (rms) streamwise velocities, $\overline{U}^*$ and u_{rms}^*, respectively, in the gap ($x/D = -1$) of and behind the cylinders at $x/D = 1.0$ and 4.0, which are within and beyond the vortex

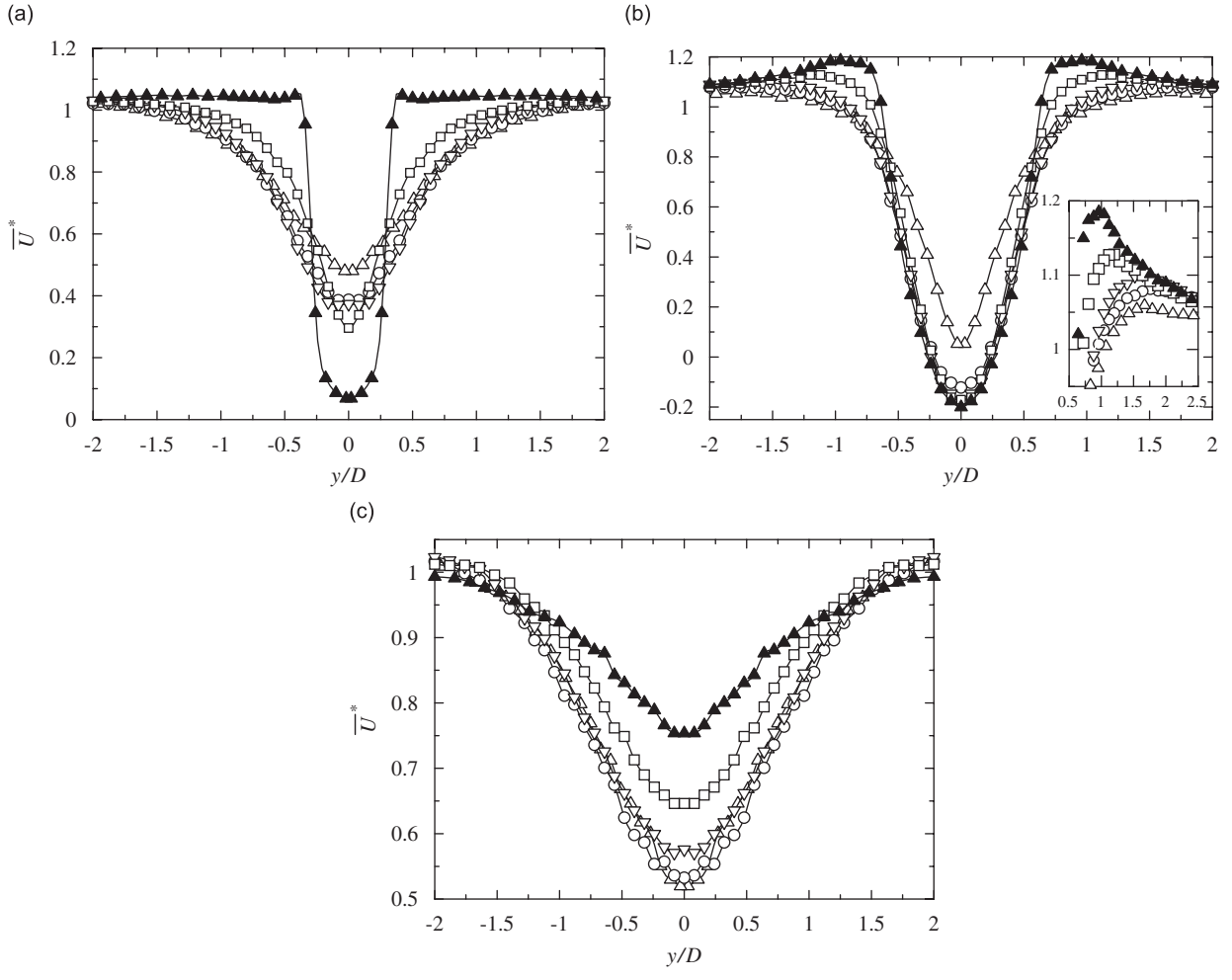

Fig. 16. Time-averaged velocity, $\overline{U}^*$, at (a) $x/D = -1.0$; (b) $x/D = 1.0$; (c) $x/D = 4.0$. △, $d/D = 1.0$; ○, $d/D = 0.8$; ∇, $d/D = 0.6$; □, $d/D = 0.4$; ▲, $d/D = 0.24$.

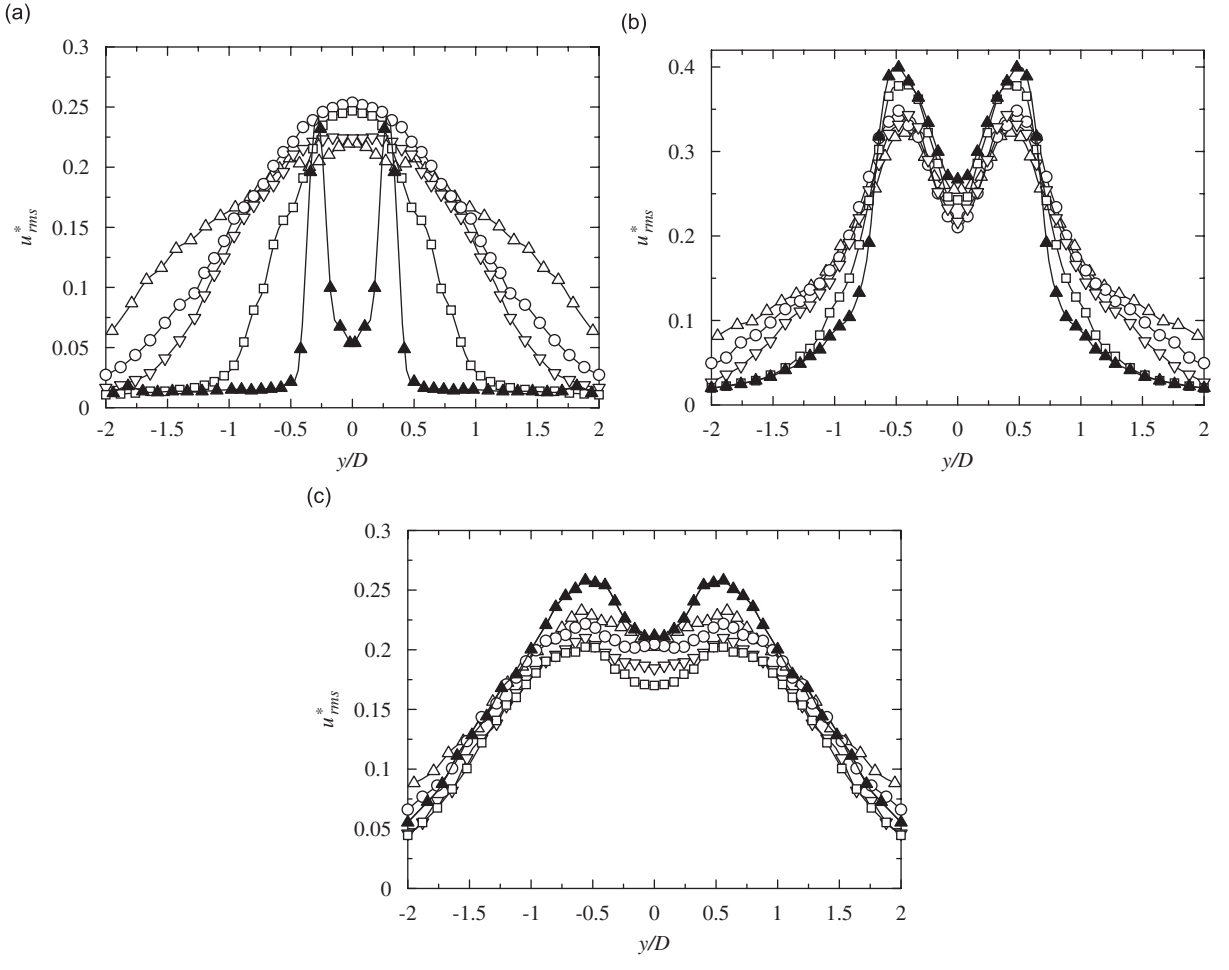

Fig. 17. Fluctuating streamwise velocity, u^*_{rms}, at (a) $x/D = -1.0$; (b) $x/D = 1.0$; (c) $x/D = 4.0$. △, $d/D = 1.0$; ○, $d/D = 0.8$; ▽, $d/D = 0.6$; □, $d/D = 0.4$; ▲, $d/D = 0.24$.

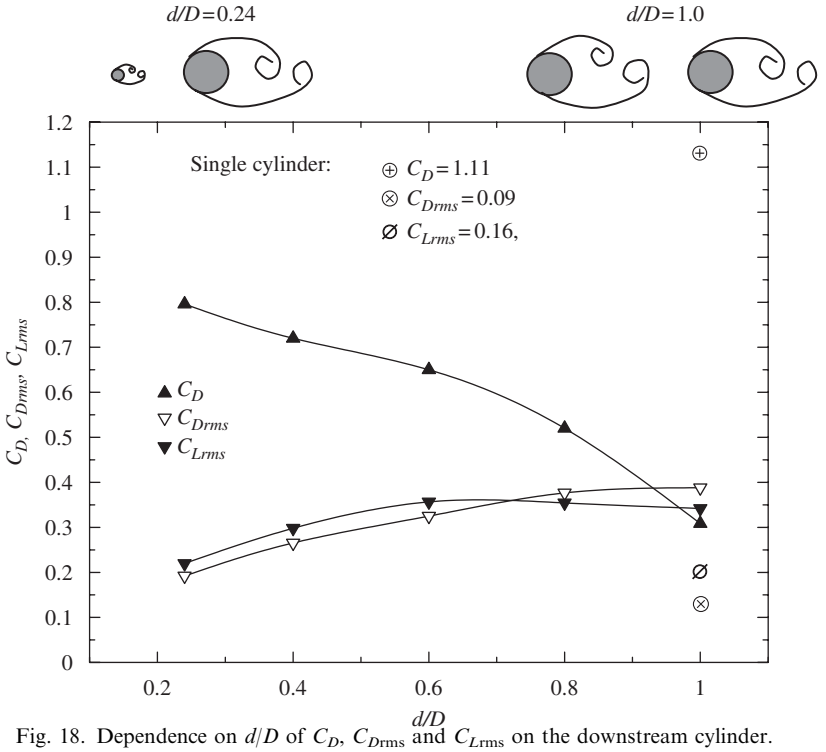

Fig. 18. Dependence on d/D of C_D, $C_{D\mathrm{rms}}$ and $C_{L\mathrm{rms}}$ on the downstream cylinder.

formation length, respectively. At $x/D = -1$, the centerline deficit $1 - \overline{U}^*$ increases with decreasing d/D (Fig. 16(a)). The same is observed at $x/D = 1.0$ (Fig. 16(b)) but the opposite occurs at $x/D = 4.0$ (Fig. 16(c)). It may be inferred from the streamwise variation of $1 - \overline{U}^*$ with d/D (Fig. 16(b, c)) that the velocity recovery rate is higher for smaller d/D, implying a higher entrainment rate of free-stream fluid into the wake (Alam and Zhou, 2007b). The observation may also suggest larger vortex strength behind the downstream cylinder and hence an increasing time-averaged drag with decreasing d/D, which will be later confirmed by measured forces on the downstream cylinder. The lateral distributions of both $\overline{U}^*$ (Fig. 16(a)) and u^*_{rms} (Fig. 17(a)) appear to be narrowing with declining d/D, suggesting a smaller wake width and vortex size in the gap between the cylinders, consistent with the observation in Fig. 12. Being within the vortex formation region, $\overline{U}^*$ at $x/D = 1.0$ (Fig. 16(b)) may represent the velocity distribution of free shear layer separating from the downstream cylinder. The maximum $\overline{U}^*$ is 1.06, 1.08, 1.10, 1.13 and 1.19 for $d/D = 1.0$, 0.8, 0.6, 0.4 and 0.24, respectively, that is, the free shear layer velocity around the downstream cylinder increases with decreasing d/D, implying an increasing time-averaged drag (Roshko, 1954). Furthermore, the $\overline{U}^*$ peak (see the insert of Fig. 16(b)) becomes narrower for smaller d/D, suggesting that the free shear layer around the downstream cylinder becomes thinner, conforming to the observation from Fig. 12. This narrowing shear layer is also evident in u^*_{rms} (Fig. 17(b)). A narrowing shear layer in general corresponds to a higher drag (Nakaguchi et al., 1968) as well as a higher Strouhal number (Roshko, 1954).

The u^*_{rms} value over $y/D = -1.0$–1.0 at $x/D = 4$ (Fig. 17(c)) decreases from $d/D = 1.0$ to 0.4 but increases from $d/D = 0.4$ to 0.24. Since vortices from the upstream cylinder impinge on the downstream cylinder, u^*_{rms} behind the downstream cylinder is expected to be dependent on the strength of the vortices and how the vortices interact with the shear layer separation from the downstream cylinder. The decrease in u^*_{rms} with decreasing d/D from 1.0 to 0.4 is probably due to the combined effect of the decreasing strength of impinging vortices and the intermittent lock-in of the two vortex shedding process. The increase of u^*_{rms} from $d/D = 0.4$ to 0.24 may be attributed to the fact that the two vortex shedding processes are not locked-in with each other at $d/D = 0.24$.

4.3. Forces on the downstream cylinder

Fig. 18 presents time-averaged drag (C_D), fluctuating drag ($C_{D\mathrm{rms}}$) and lift ($C_{L\mathrm{rms}}$) on the downstream cylinder. It is well known that $C_{D\mathrm{rms}}$ and $C_{L\mathrm{rms}}$ on a cylinder are highly dependent on oncoming flow conditions. For example, $C_{D\mathrm{rms}}$

and $C_{L\mathrm{rms}}$ decrease with increasing turbulent intensity (Surry, 1972; Laneville et al., 1975; Nakamura and Ohya, 1984), but increase with the increasing strength of oncoming vortices (Gursul and Rockwell, 1990; Lee and Smith, 1991; Rockwell, 1998; Alam et al., 2003a, 2005, 2006). The value of C_D increases with decreasing d/D from 1.0 to 0.24, apparently linked to the increasing approaching flow velocity to the downstream cylinder. The increasing value of C_D with decreasing d/D from 1.0 to 0.24 is consistent with increasing centerline velocity deficit (Fig. 16(b)), narrowing shear layer thickness (Figs. 16(b), 17(b)) and increasing shear layer velocity (Fig. 16(b)). On the other hand, $C_{D\mathrm{rms}}$ and $C_{L\mathrm{rms}}$ decrease for a smaller d/D due to a decrease in the strength of oncoming vortices although the increasing approaching flow velocity may increase $C_{D\mathrm{rms}}$ and $C_{L\mathrm{rms}}$.

5. Conclusions

The wake of two tandem cylinders of different diameters has been experimentally investigated, including the flow structure, Strouhal numbers and forces. The flow is in the co-shedding regime ($L/d = 5.5$); the diameter ratio is from 1 to 0.24. The investigation leads to the following conclusions:

1. One dominant frequency only occurs between the cylinders. However, two are detected behind the two cylinders, including the case of $d/D = 1.0$, which has not been previously reported. One is identical to that of vortex shedding from the upstream cylinder, and the other is ascribed to vortex shedding from the downstream cylinder. The frequency of vortex shedding from the downstream cylinder is lower than that from the upstream cylinder, but the two are intermittently the same, or 'locked-in', for $d/D \geqslant 0.4$. While the vortices of the higher frequency decay rapidly behind the downstream cylinder, those of the lower grow all the way to the farthest downstream distance, i.e., $x/D = 22$, presently examined. Both LIF flow visualization and PIV capture two distinct flow structures behind the downstream cylinder under the same experimental conditions, one displaying a higher-frequency vortex street that disappears at $x/D > 5$ and the other a lower-frequency street, which is consistent with the analysis of the dominant vortex frequencies. The intermittent lock-in is not observed for $d/D < 0.4$.
2. The dimensionless frequency, St_d, of vortex shedding from the upstream cylinder declines progressively from 0.196 at $d/D = 1$ to 0.173 at $d/D = 0.24$, probably because the downstream cylinder acts to slow down the flow around the upstream cylinder. On the other hand, the dimensionless frequency, St_D, of vortex shedding from the downstream cylinder increases from $= 0.12$ at $d/D = 1$ to 0.203 at $d/D = 0.24$ due to an increase in the incident flow velocity to this cylinder.
3. With decreasing d/D, the time-averaged drag on the downstream cylinder increases, due to less stagnant fluid or larger dynamic pressure between cylinders. However, the fluctuating forces on this cylinder drop because a smaller d/D should result in the impaired strength of vortex shedding from the upstream cylinder.
4. As d/D decreases, the width of the wake between the cylinders appears to narrow. Furthermore, the centerline deficit $1 - \overline{U}^*$ at $x/D = 1$ behind the downstream cylinder increases for smaller d/D, and the velocity recovery rate is higher, implying a higher entrainment rate due to stronger vortices. The results are internally consistent with the observed dependence of the time-averaged drag on d/D.
5. At very small d/D, 0.4 or smaller, the frequency of vortex shedding from the upstream cylinder may be measured in the gap of the two cylinders, but not behind. As a matter of fact, the Strouhal number, time-averaged drag, and fluctuating drag and lift associated with the downstream cylinder all approach their counterparts in an isolated cylinder wake, implying a negligibly small effect of the upstream cylinder on the downstream cylinder wake.

Acknowledgments

Y.Z. wishes to acknowledge support given to him by the Research Grants Council of the Government of the HKSAR through Grants PolyU B-Q862.

References

Alam, M.M., Sakamoto, H., 2005. Investigation of Strouhal frequencies of two staggered bluff bodies and detection of multistable flow by wavelets. Journal of Fluids and Structures 20, 425–449.

Alam, M.M., Zhou, Y., 2007a. Phase lag between vortex sheddings from two tandem bluff bodies. Journal of Fluids and Structure 23 (2), 339–347.

Alam, M.M., Zhou, Y., 2007b. The turbulent wake of an inclined cylinder with water running. Journal of Fluid Mechanics 589, 261–303.

Alam, M.M., Moriya, M., Takai, K., Sakamoto, H., 2003a. Fluctuating fluid forces acting on two circular cylinders in a tandem arrangement at a subcritical Reynolds number. Journal of Wind Engineering and Industrial Aerodynamics 91, 139–154.

Alam, M.M., Moriya, M., Sakamoto, H., 2003b. Aerodynamic characteristics of two side-by-side circular cylinders and application of wavelet analysis on the switching phenomenon. Journal of Fluids and Structures 18, 325–346.

Alam, M.M., Sakamoto, H., Moriya, M., 2003c. Reduction of fluid forces acting on a single circular cylinder and two circular cylinders by using tripping rods. Journal Fluids and Structures 18, 347–366.

Alam, M.M., Sakamoto, H., Zhou, Y., 2005. Determination of flow configurations and fluid forces acting on two staggered circular cylinders of equal diameter in cross-flow. Journal of Fluids and Structures 21, 363–394.

Alam, M.M., Sakamoto, H., Zhou, Y., 2006. Effect of a T-shaped plate on reduction in fluid forces acting on two tandem circular cylinders in a cross-flow. Journal of Wind Engineering and Industrial Aerodynamics 94, 525–551.

Daubechies, I., 1990. The wavelet transform, time-frequency localization and signal analysis. IEEE Transaction, Information Theory 36, 961–1005.

Farge, M., 1992. Wavelet transforms and their applications to turbulence. Annual Review of Fluid Mechanics 24, 395–457.

Gursul, I., Rockwell, D., 1990. Vortex-street impinging upon an elliptical leading edge. Journal of Fluid Mechanics 211, 211–242.

Hamdan, M.N., Jubran, B.A., Shabaneh, N.H., Abu-Samak, M., 1996. Comparison of various basic wavelets for the analysis of flow-induced vibration of a cylinder in cross-flow. Journal of Fluids and Structures 10, 633–651.

Huang, J.F., Zhou, Y., Zhou, T.M., 2006. Three-dimensional wake structure measurement using a modified PIV technique. Experiments in Fluids 40, 884–896.

Igarashi, T., 1984. Characteristics of the flow around two circular cylinders arranged in tandem (2nd report). Bulletin of the Japan Society of Mechanical Engineering 27, 2380–2387.

Ishigai, S., Nishikawa, E., Nishimura, E., Cho, K., 1972. Experimental study of structure of gas flow in tube banks axes normal to flow. Bulletin of the Japan Society of Mechanical Engineering 15, 949–956.

King, R., Johnes, D.J., 1976. Wake interaction experiments with two flexible circular cylinders in flowing water. Journal of Sound and Vibration 45, 259–283.

Kiya, M., Arie, M., Tamura, H., Mori, H., 1980. Vortex shedding from two circular cylinders in staggered arrangement. ASME Journal of Fluids Engineering 102, 166–173.

Laneville, A., Gartshore, I.S., Parkinson, G.V., 1975. An explanation of some effects of turbulence on bluff bodies. In: Proceedings of Fourth International Conference on Winds Effects on Building and Structures, Heathrow, England, K75-363, pp. 333–341.

Lee, D.J., Smith, C.A., 1991. Effect of vortex core distortion on blade-vortex interaction. AIAA Journal 29, 1355–1363.

Lee, S.J., Lee, S.I., Park, C.W., 2004. Reducing the drag on a circular cylinder by upstream installation of a small control rod. Fluid Dynamics Research 34, 233–250.

Li, H., 1997. Wavelet auto-correlation analysis applied to eddy structure identification of free turbulent shear flow. International Journal of the Japan Society of Mechanical Engineers 40, 567–576.

Meneghini, J.R., Saltara, F., Siqueira, C.L.R., Ferrari Jr., J.A., 2001. Numerical simulation of flow interference between two circular cylinders in tandem and side-by-side arrangement. Journal of Fluids and Structures 15, 327–350.

Nakaguchi, H., Hasimoto, K., Muto, S., 1968. An experimental study of aerodynamic drag on rectangular cylinders. Japan Society of Aeronautical Space Science 16, 1–5.

Nakamura, Y., Ohya, Y., 1984. The effects of turbulence on the mean flow past a two-dimensional rectangular cylinders. Journal of Fluid Mechanics 149, 255–273.

Newland, D.E., 1993. An Introduction of Random Vibrations, Spectral and Wavelet Analysis, third ed. London, Longman Scientific and Technical.

Rinoshika, A., Zhou, Y., 2005a. Effects of initial conditions on a wavelet-decomposed turbulent near-wake. Physical Review E 71, 057504:1-8.

Rinoshika, A., Zhou, Y., 2005b. Orthogonal wavelet multi-resolution analysis of a turbulent cylinder wake. Journal of Fluid Mechanics 524, 229–248.

Rockwell, D., 1998. Vortex-body interactions. Annual Review of Fluid Mechanics 30, 199–229.

Roshko, A., 1954. On the drag and shedding frequency of two-dimensional bluff bodies. NACA Technical Note No. 3169.

Sakamoto, H., Haniu, H., Obata, Y., 1987. Fluctuating forces acting on two square prisms in a tandem arrangement. Journal of Wind Engineering and Industrial Aerodynamics 26, 85–103.

Sakamoto, H., Takeuchi, N., Haniu, H., Tan, K., 1997. Suppression of fluid forces acting on square prism by passive control. Journal of Fluids Engineering 119, 506–511.

Strykowski, P.J., Sreenivasan, K.R., 1990. On the formation and suppression of vortex 'shedding' at low Reynolds numbers. Journal of Fluid Mechanics 218, 71–107.

Surry, D., 1972. Some effects of intense turbulent on the aerodynamic of a circular cylinder at subcritical Reynolds number. Journal of Fluid Mechanics 52, 543–563.

Torrence, C., Compo, G., 1998. A practical guide to wavelet analysis. Bulletin of the American Meteorological Society 79, 61–78.

West, G.S., Apelt, C.J., 1993. Measurements of fluctuating pressures and forces on a circular cylinder in the Reynolds number range 10^4 to 2.5×10^5. Journal of Fluids and Structures 7, 227–244.

Xu, G., Zhou, Y., 2004. Strouhal numbers in the wake of two inline cylinders. Experiments in Fluids 37, 248–256.

Yilmaz, T., Kodal, A., 2000. An analysis on coaxial jet flows using different decomposition techniques. Journal of Fluids and Structures 14, 359–373.

Yong, R.K., 1998. Wavelet Theory and Its Application, sixth ed. Kluwer Academic Publishers, USA.

Zdravkovich, M.M., 1987. The effects of interference between circular cylinders in cross flow. Journal of Fluids and Structures 1, 239–261.

Zdravkovich, M.M., 1997. Flow Around Circular Cylinders, vol. 1. Fundamentals, Oxford Science Publications.

Zhou, Y., Yiu, M.W., 2006. Flow structure, momentum and heat transport in a two-tandem-cylinder wake. Journal of Fluid Mechanics 548, 17–48.